Applied Catalysis B: Environmental 178 (2015) 192–200

Contents lists available at ScienceDirect

Applied Catalysis B: Environmental

journal homepage: www.elsevier.com/locate/apcatb

Photocatalytic films for soil fumigation: Control of dimethyl disulfide concentration after fumigation

M. Le Bechec[a], N. Costarramone[a], T. Fouillet[b], P. Charles[b], T. Pigot[a], D. Bégué[a], S. Lacombe[a,*]

[a] IPREM UMR CNRS 5254 Université de Pau et des Pays de l'Adour, Hélioparc, 2 avenue du Président Angot, 64053 Pau Cedex 09, France
[b] ARKEMA France Groupement de Recherches de Lacq, Service Thiochimie et Chimie Fine – TCF, RD 817 BP 34, 64170 Lacq, France

ARTICLE INFO

Article history:
Received 16 June 2014
Received in revised form 7 September 2014
Accepted 8 September 2014
Available online 16 September 2014

Keywords:
Dimethyldisulfide
Photocatalysis
Virtually impermeable film
Fumigation
Titanium dioxide

ABSTRACT

The photocatalytic oxidation of dimethyl disulfide (DMDS), a large spectrum and efficient fumigant, was studied with newly developed industrial Virtually Impermeable Films including a photocatalytic function. The aim was to define the optimal film composition to decrease DMDS concentration in the air space between the soil and the film at the end of the treatment while keeping an optimal DMDS concentration during the fumigation treatment. From the comparison between various films with different composition (polyethylene (PE) and polyamide (PA) layers together with a photocatalytic layer), number of layers, thickness and TiO_2 concentration, it was concluded that for all the samples the light absorption was linearly correlated to TiO_2 surface density. The optimal TiO_2 content for efficient (98%) light absorption was determined.

A first screening of the films was first carried out on the photocatalytic oxidation of acetone. Different diffusion rates of acetone and DMDS inside the PE matrix were deduced from the comparison of the results with the colored black and white films. Complete mineralization of acetone and less extensive mineralization of DMDS (due to formation of methanesulfonate together with sulfates) was observed with most of the studied films. Colored black and white films with suitable design were also efficient for DMDS degradation, but not for acetone mineralization.

Since it is known that DMDS and its oxidation products are beneficial for plant growth, it was concluded that colored or uncolored gastight photocatalytic films could be successfully used for wide field fumigation with DMDS by optimizing its degradation rate in the air space for maximum nematicide, fungicide and herbicide efficiency, with decreased buffer zones (area of no fumigation) and maximum safety for neighborhood and workers at the end of the treatment.

1. Introduction

Soil fumigation is needed to control a broad range of soil borne disease such as nematodes, bacteria, fungi and weeds that affect production of many high-value crops (*e.g.* tomato, strawberry and pepper). The soil fumigation was initiated in 1869 with the use of carbon disulfide (CS_2) as the *Phylloxera vitifoliae* control product [1]. Afterwards, alternative volatile molecules like Methyl Bromide (MB), 1,2-dibromo-3-chloropropane (DBCP), ethylene dibromide (EDB), Chloropicrin (CP), 1,3-dichloropropene (1,3-D) and methylisocyanate (MITC) generator such as metam sodium were used. CS_2 is a broad range biocide but because of its relatively high treatment rates and high toxicity, flammability and cost, its use is now forbidden in most countries. The discovery of DBCP and EDB in groundwater in California led to withdraw these later fumigants from the market in the 80s. In 1997, the Montreal Protocol called for phase out of MB because of its stratospheric ozone-depleting effect [2]. Several other products like CP or MITC have recently been labeled as "restricted use pesticides" due to their acute toxicity. This led to the emergence of alternative molecules such as dimethyl disulfide (DMDS) [3].

Generally fumigants are injected into the soil before planting by drip or shank injection. Soil fumigation is a complex dynamic process influenced by many factors such as soil type and texture, moisture, temperature, organic matter but also volatility, stability and bio degradation of the fumigants. The important issue to remove or strongly decrease the level of pests is to maintain an optimal concentration during an optimal time.

* Corresponding author. Tel.: +33 559 407 579.
E-mail address: sylvie.lacombe@univ-pau.fr (S. Lacombe).

http://dx.doi.org/10.1016/j.apcatb.2014.09.022
0926-3373/

The global trend in developed countries is to limit levels of fumigants to preserve the environment and workers, field's residents and consumers' health. One solution is to cover fields with gastight plastic films after fumigation [4–6]. This allows maintaining the same local concentration with less amount of fumigant by limiting its dissemination in the atmosphere. Current agriculture practice has used for a long time low-density polyethylene films (LDPE) that provide good moisture barrier for mulching and broadcasting. Standard transparent or colored polyethylene (PE) films are typically made of 2 or 3 layers of PE. Uncolored plastic agricultural films were primary used to increase the soil temperature and thus the crops' germination. Black films allowed early crop rising by combining two effects: heating the ground and limiting weeds rising. On the contrary, white films were used to reduce ground heating by reflecting the solar emission. However these films were generally permeable to organic vapor and so did not strongly reduce the global fumigant emission into the atmosphere [4].

To improve the tightness of the films to the fumigants, impermeable films (virtually impermeable films, VIF, and totally impermeable films, TIF) were developed by adding to several PE layers an intermediate impermeable one containing ethylene vinyl alcohol (EVOH) or polyamides (PA). Several studies were led in laboratory and in full fields with several PE films to monitor fumigants dispersal in air and soil. The efficiency of these films depended on their permeability against a given fumigant but also on the temperature, the soil moisture and the ground texture [7]. Nevertheless, impermeable films improved ground disinfection relative to LDPE. After the fumigation step, these VIF films could also be let on the ground and punched out to plant various crops and thus optimized the germination step. But cutting a tight film after fumigation could also expose workers to residual chemical vapors.

To address this drawback, a new generation of fumigation films were developed by combining photocatalysis and impermeable films [8]. Actually, photocatalysis has been known for a long time to oxidize many organic compounds in water or air by using a semi-conductor like TiO_2 under solar light [9,10]. Unlike photocatalysis in solution where TiO_2 nanoparticles are generally dispersed in water, for gas phase oxidation, the semi-conductor has to be immobilized. In this later case, the crucial points to achieve good photocatalytic efficiency are the contact between the pollutant and the photocatalyst and the proper irradiation of the catalyst particles. Polymeric materials present several advantages as TiO_2 support: they are easily shaped, UV-transparent and able to embed TiO_2 nanoparticles. Such materials were successfully tested for depollution [11–15] and for bactericidal properties in food packaging [16,17]. Besides their activity against pollutants, these materials also demonstrated self-oxidation and auto-degradation under UV as expected with an organic TiO_2 support [18].

In this work, we have tested VIF type photocatalytic films, developed by Arkema France, in order to suppress the emission of fumigants in the atmosphere at the end of the fumigation period. These uncolored and colored VIF films containing a photocatalytic layer were tested at the laboratory scale. For quick screening of the efficiency of the films, acetone mineralization in a 1.2 m^3 closed chamber was chosen according to the normalized AFNOR standard XP B44-013 for air cleaning efficiency. Another set of tests with DMDS in a smaller closed chamber was then carried out without any optimization of mass transfer to better fit with the actual field conditions. Nano sized TiO_2 P25® (Evonik) was embedded into a PE layer at several concentrations and the influence of the film thickness and of the possible addition of a colored layer on the photocatalytic properties was investigated.

2. Materials and methods

2.1. Description of the films and characterization methods

Nine photocatalytical VIF films with 3, 4 or 5 layers were elaborated according to the previous patent [8]. A first UV-transparent PE layer (1 in Fig. 1) gave films their mechanical resistance. The second polyamide layer (PA, 2) was virtually impermeable to the fumigant, UV transparent and between 6 to 15 μm thick. The third PE layer (3) contained the catalyst (TiO_2) allowing the diffusion of the fumigant. The mineral catalyst (P25® Evonik 70% anatase, 30% rutile) was integrated into the polymer matrix by diluting a previously prepared master batch, giving a better TiO_2 dispersion into the PE matrix. The optimal incorporation of photocatalyst in the polymer matrix was obtained with the master batch technic: a blend was prepared with at least one polymer and the mineral photocatalyst at a concentration between 10 and 50% of total mass and extruded with a single screw extruder, without any complementary additive. The photocatalytic layer was prepared by dilution of the master batch in the polyolefin matrix in order to obtain a final concentration of catalyst between 5 and 50% of total mass [8]. The good dispersion of photocatalyst was function of the profile of the screw, the final concentration of photocatalyst and the melt index of the polymer matrix. This method allowed well-dispersed photocatalytic layer preparation without any modification of the production line. The samples T3L/13/3MB1 and T3L/13/3MB2 were produced at different time with the same photocatalyst and the same method.

The final mass concentration of TiO_2 in this layer was between 1 and 4.5% and its thickness was between 15 and 50 μm. An optional layer (4), colored with white (pigmentary TiO_2) or black (carbon black) pigment, could be added at the bottom of the film. At this position, the absorption of light by the pigment layer did not prevent the UV activation of the catalyst in the upper layer (3). In the

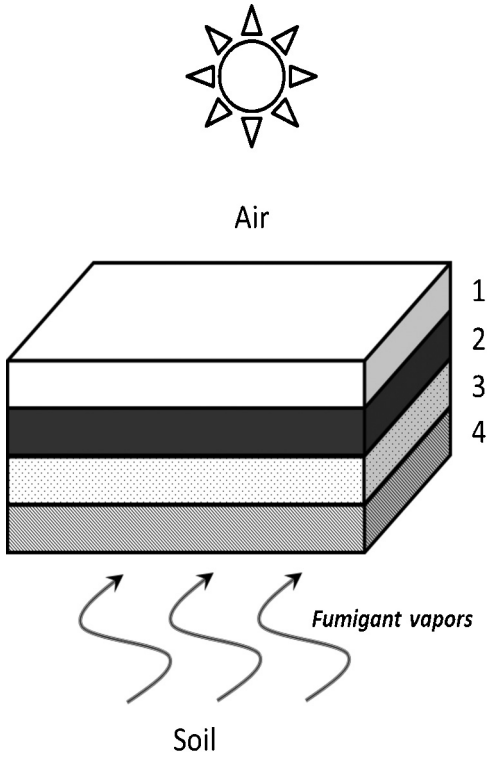

Fig. 1. Scheme of the VIF photocatalytic film architecture: 1, UV transparent PE layer; 2, polyamide impermeable layer; 3, PE layer with TiO_2; 4, optional colored PE layer.

Table 1
Film composition, thickness and TiO_2 surface density. In column 2: PE layer/polyamide layer (in bold characters)/PE TiO_2 layer (in underlined characters)/optional colored PE layer (in italic bold characters) (mass percent of TiO_2 in the photoactive layer). MB1 and MB2 for two different master batches.

Name	Detailed thickness/μm and (% of TiO_2 in mass)	Total thickness/TiO_2 layer thickness (μm)	TiO_2 surface density ($g\,cm^{-2}$)
T3L/13/0	13/**6**/13	32/13	0
T3L/13/1	13/**6**/13 (1.0%)	32/13	1.21×10^{-5}
T3L/13/3MB1	13/**6**/13 (3.0%)	32/13 (MB1)	3.63×10^{-5}
T3L/13/3MB2	13/**6**/13 (3.0%)	32/13 (MB2)	3.63×10^{-5}
W4L/13/3	13/**6**/13/***5***5 (3.0%)	37/13	3.63×110^{-5}
B5L/13/3	13/**10**/5/13/***5*** (3.0%)	46/13	3.63×110^{-5}
T3L/50/1.3	15/**15**/50 (1.3%)	80/50	6.05×10^{-5}
T3L/15/4.5	15/**10**/15 (4.5%)	40/15	6.28×10^{-5}
T3L/50/3.3	15/**15**/50 (3.3%)	80/50	1.53×10^{-4}

following, the films are named according to their color (T transparent, W white and B black), the number of layers (3–5 L), the thickness of the photocatalytic layer (10.5–50 μm) and the mass percent of TiO_2 in the photoactive layer (1–4.5%). Some parameters of the films were studied such as the master batch nature (T3L/13/3MB1 and T3L/13/3MB2) and assembly processes of the films (T3L/15/4.5 and T3L/10.5/3).

To compare the films, we calculated their TiO_2 surface density: given the PE density ($0.93\,g\,cm^{-3}$) and the thickness of the PE TiO_2 layer, the mass of PE per cm^2 may be determined and according to the weight percent TiO_2 in this layer, the TiO_2 mass per cm^2 was deduced assuming that the low amount of TiO_2 did not modify the PE density. In the following (Table 1), the detailed films composition is represented by 3 or 4 successive numbers corresponding successively to the thickness of: PE layer (1 in Fig. 1), polyamide layer (2) in bold characters, PE TiO_2 layer (3) in underlined characters and the optional italic bold PE layer (4) in colored characters. Only white colored W4L/13/3 (PE/PA/PE TiO_2/white colored PE) and black B5L/13/3 (PE/PA/PE/PE TiO_2/black colored PE) colored films contained additional PE layers below the photocatalytic layer. White colored PE included white pigmentary TiO_2 (PB 8000, Schulman) and the black one included carbon black (Polyblack 1420, Schulman).

Scanning electron microscopy images were recorded with a Scanning Electron Microscope (SEM) ZEISS Leo type 1530 model VP (FEG, resolution 1 nm at 20 kV and 3 nm at 3 kV) in the high vacuum mode at a tension of 1.3 or 10 kV with the secondary electron detector. X analysis was carried out with an X-rays analyzer OXFORD type "Energy 200"(resolution 138 ev) at a tension of 10 kV. Transmission electronic microscopy (TEM) was carried out with a Philips CM200 microscope, 200 kV, filament LaB6, resolution 0.25 nm. The UV transmission spectra of the films were recorded with a Perkin-Elmer 860 double beam spectrophotometer equipped with a 15 cm diameter-integrating sphere bearing the sample holder in the vertical position. They were recorded at room temperature in step of 1 nm in the range of 250–600 nm with a bandwidth of 2 nm. The instrument was calibrated with a certified Spectralon white standard (Labsphere, North Sutton, USA).

XPS measurements on the irradiated films were performed on a Thermo K-alpha spectrometer with a hemispherical analyzer and a microfocussed (analysis area *ca.* 400 mm^2) monochromatized radiation (AlKα, 1486.6 eV) operating at 72 W under a residual pressure of 10^{-9} mbar. The pass energy was set to 20 eV. Charge effects were compensated by the use of a dual beam charge neutralization system (low energy electrons and Ar^+ ions). All the neutralizer parameters remained constant during analysis and allow ones to find a 285.0 eV C1s binding energy for adventitious carbon. Spectra were mathematically fitted with Casa XPS software using a least squares algorithm and a nonlinear baseline. The fitting peaks of the

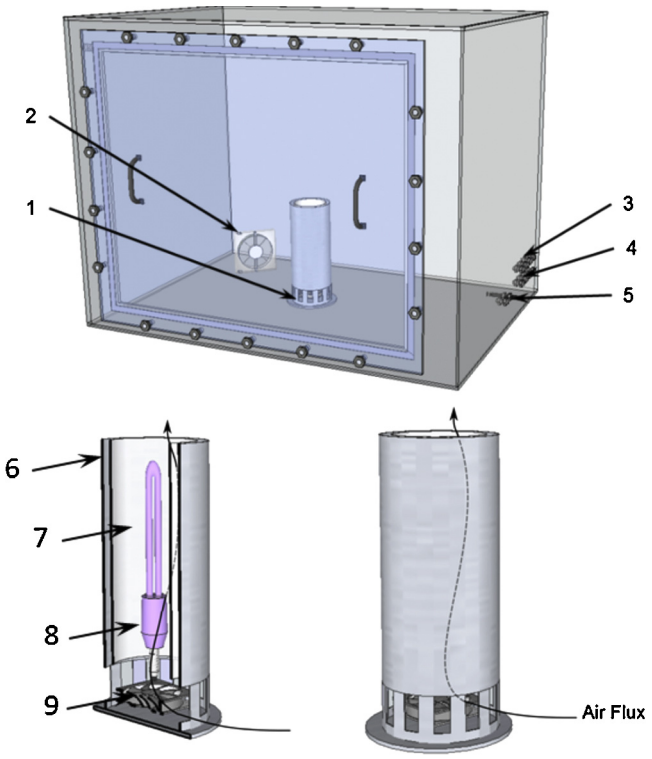

Fig. 2. (A) 1.17 m^3 closed chamber used for the photocatalytic tests with acetone. (B) Photocatalytic device with the film. 1: photocatalytic device; 2: homogenization fan; 3: on line GC analysis; 4: sypac pumping system; 5: T & %HR sensor; 6: external sheath; 7: film; 8: UV light; 9: fan (pictures of the devices in ESI, Fig. S2).

experimental curves were defined by a combination of Gaussian (70%) and Lorentzian (30%) distribution.

2.2. Photocatalytic tests

Photocatalytic tests with acetone (50 ppmV, normal conditions) as a model volatile organic compound (VOC) were carried out in a 1.17 m^3 closed chamber (Fig. 2) as described by Kartheuser et al. [19] and developed for the AFNOR standard XP B44-013. The control of the chamber tightness without any photocatalytic system showed that less than 8% of variation of COV concentration was observed within 8 h. A sheet of film (30 cm × 20 cm) was placed in a photocatalytical device at 2 cm distance around a UV lamp (Sylvania 20WBL368 UVA delivering $10\,mW\,cm^{-2}$ of total light and $6.6\,mW\,cm^{-2}$ of UVA). A $20\,m^3\,h^{-1}$ fan was placed in the bottom of this device to force the contact of the pollutant with the film. The chamber was first flushed with dried air without CO_2 and then with humid air without CO_2 to obtain 50 ± 5% of relative humidity (RH) at 22 °C. The chamber was equipped with an air homogenization system (external fan) with a maximum flow $120\,m^3\,h^{-1}$. Temperature and humidity were recorded during all the experiment. Known amount of acetone (50 ppmV) was injected through a septum. VOC and CO_2 concentrations were determined by automatic sampling with a GC-FID, GC-PID and GC-methanizer-FID during 24 h of test.

Photocatalytical tests with dimethyl disulfide (DMDS) were carried out in a smaller tight box (144 L) equipped with two homogenization fans and an upper pyrex window (Fig. 3). A 20 cm × 20 cm sheet of films was fixed 5 cm from the pyrex window. Four UV lamps (Philips TLD15W05) delivering $4\,mW\,cm^{-2}$ UVA at the film position were placed over the glass window. The box was first flushed with clean air (without CO_2) saturated with water (70% at 20 °C). 100 ppmV of DMDS (normal conditions) were injected though a septum. DMDS and CO_2 concentrations were

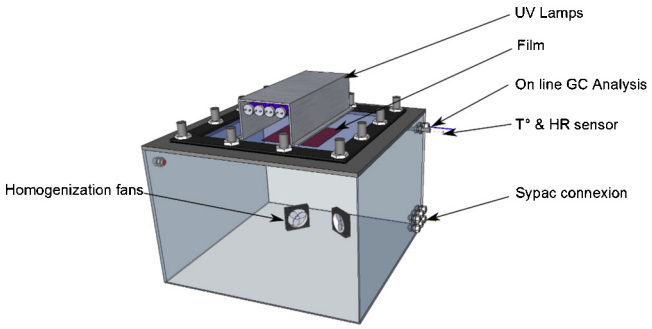

Fig. 3. 144 L tight box used for photocatalytic tests against DMDS with two homogenization fans and an upper Pyrex window on which the lamps were placed and below which the film was hold (pictures of the device in ESI, Fig. S3).

recorded by automatic sampling with a GC-TCD (Varian CP4900). The by-products could be analyzed by ATD-GC-MS after an adsorption step on Air Toxic cartridges (PerkinElmer) with a Sypac pumping system (Tera Environnement). A previous validation step of the setup showed that less than 5% of DMDS was lost in 24 h without any film. The experimental procedure started with a first step without DMDS to control any VOC and CO_2 released by the film under UV exposure during 60 h. This gave the rate of CO_2 and by-products emitted by auto-oxidation of the photocatalytic film. The second step with 100 ppmV DMDS was carried out for 60 h.

Light sources irradiance was measured with a calibrated spectroradiometer AVASPEC 2048 L. The 3.9 mm diameter sensor was placed at the exact position of the film (irradiance of both used lamps in ESI, Fig. S1). The measured irradiance in the DMDS experiment (small chamber) was of the same order of magnitude as the solar exposure (5.4 mW cm^{-2} in July in Paris [20]).

In both cases, after sampling with "Air toxic" cartridge (PerkinElmer), the adsorbed VOC were desorbed at 320 °C with a PerkinElmer Turbo matrix 650 Thermal Desorber. VOC were then injected to the PerkinElmer Clarus 680 Gas Chromatograph and separated. The VOC were characterized with a Clarus 600 Mass Spectrometer.

The sulfates and methane sulfonates adsorbed on the films were analyzed by ionic chromatography after washing the sheets of films with known volumes of water. After a 100-fold dilution in deionized water, the samples were analyzed by ionic chromatography (ICS3000 Dionex) with a pre-column AG15, a column As15 (Dionex) and NaOH as mobile phase.

3. Results

3.1. Films characterization

Cross sections of the films were observed by SEM pictures, which showed well defined layers whose thickness were in good agreement with specifications. The X analysis showed titania peaks only in the photocatalytic layer ((3) in Fig. 1) for all the three-layered samples and in the photocatalytic layer (3) and colored layer (4) for the white four-layered sample W4L/13/3 shown in Fig. 4A. Actually in this later case, the white pigment is pigmentary TiO_2 (masterbatch PB white 8000 from Schulman). In all the other layers, only carbone and oxygen peaks were observed, meaning that TiO_2 was well mixed with the PE matrix and did not diffuse in the other layers. TEM microscopy revealed agregates (about 100 nm) of small nanoparticles (20 nm) of TiO_2. In the pigmentary layer (4) of the white sample (W4L/13/3) only larger TiO_2 particle (200 nm) were observed, while in the pigmentary layer (4) of the black sample (B5L/13/3) only carbon and oxygen were detected. It may be concluded than the master batch preparation led to homogenous dispersion of TiO_2 nanoparticles in the photoactive layer.

The total transmission UV spectra of the films were recorded with an integrating sphere in order to take into account light scattering by the films (Fig. 5). First, the VIF film T3L/13/0 without TiO_2 is totally transparent up to 300 nm in agreement with the absorbtion spectra of PE and polyamide. As soon as TiO_2 is incorporated in the PE layer, an absorption band in the range of 300–400 nm is clearly observed. As expected, the black film B5L/13/3 is not transparent at all and absorb all the light between 250 and 600 nm. The absorbtion band of the white film W4L/13/3 is clearly shifted to 400 nm (due to a supplementary pigmentary TiO_2 layer) and its

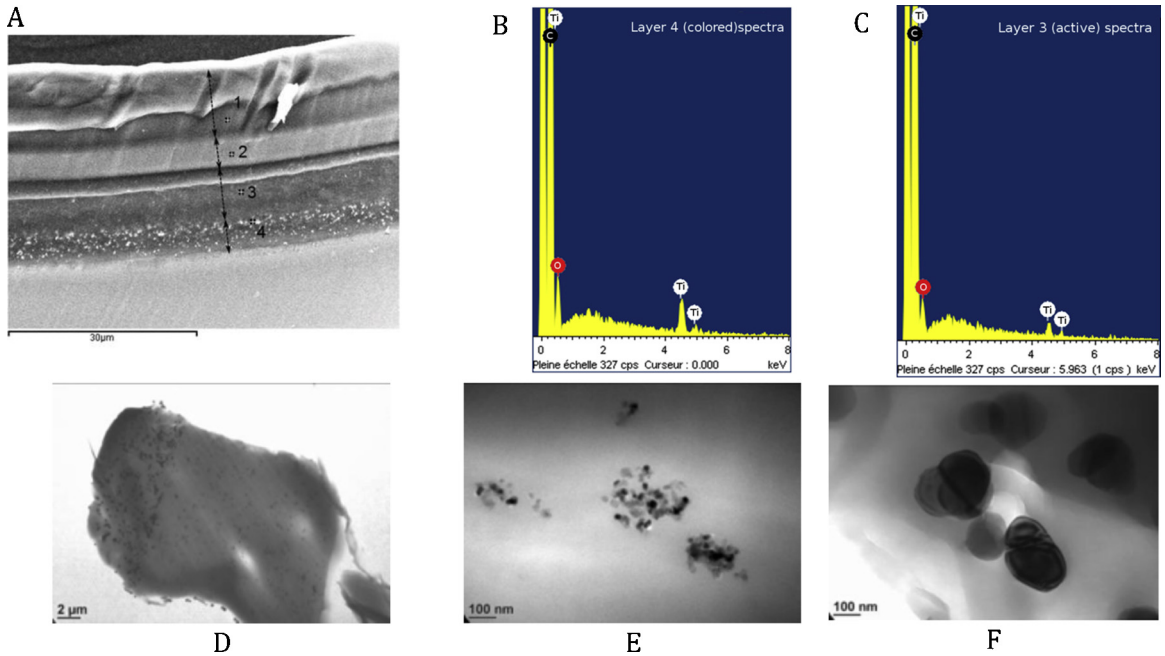

Fig. 4. Characterization of the film W4L/13/3 (A) by scanning electronic microscopy, (B) by X-ray analysis of layers (4) and (C) (3); (D) by transmission electronic microscopy; (E) zoom of particles in layer (3) with nanosized TiO_2 and (F) of layer (4) with pigmentary TiO_2.

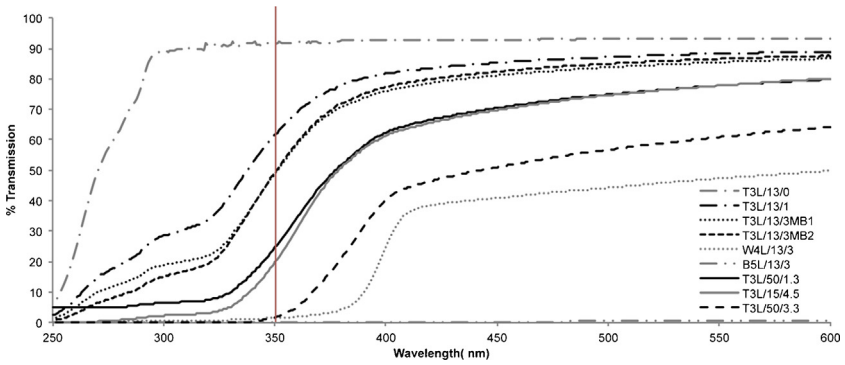

Fig. 5. Transmission spectra of the films.

total transmission is in the range 40–50% between 400 and 600 nm. This decreased transmission stems from increased light scattering of this sample relative to the other ones in the integrating sphere. In Fig. 6, the intensity of the absorption band of the transparent films at 350 nm is satisfactorily correlated with the previously described TiO_2 surface density. It may be concluded that for a TiO_2 surface density of 1.5×10^{-4} g cm^{-2} the absorbance is 1.8, meaning first, that the transmission will be about 1% and second, that under these conditions all the light will be absorbed on the whole thickness of the film. Accordingly, further increase of TiO_2 content could not be detected in the UV spectra and would not be worth due to the saturation of light absorption.

3.2. Photocatalytic results

A first screening of the films was made by studying acetone mineralization in the large volume closed chamber. For each film, a first irradiation without added acetone in air without CO_2 at 50% RH was first carried out to monitor the decomposition of the film induced by the presence of TiO_2 in the PE layer (Fig. 7B, open squares). As expected [18], a significant CO_2 evolution was observed and CO_2 concentration increased linearly with time indicating an apparent zero order kinetic whose constant k_{CO_2} could be determined ($k_{CO_2} = 0.212$ ppm Vmin^{-1}). After 24 h irradiation, the chamber was flushed with new synthetic air without CO_2 and relative humidity was adjusted to 50%. During the second experiment 50 ppmV of acetone was introduced and after an equilibration step, a second irradiation started. CO_2 concentration also increased linearly but faster than previously ($k_{CO_2} = 0.279$ ppm Vmin^{-1}, Fig. 7B, black squares). At the same time, acetone concentration decreased linearly (Fig. 7A) and the apparent zero order kinetic constant was also determined ($k_{acetone} = 0.027$ ppmV min^{-1}). If complete acetone mineralization was assumed, each mole of acetone should give 3 moles of CO_2 and this calculation led to a much slower CO_2 increase than actually observed (Fig. 7B, cross): $k_{CO_2\ theo} = 0.076$ ppmV min^{-1}. When adding this latter theoretical curve to the CO_2 curve obtained without acetone (Fig. 7B, dotted line), a good correlation with CO_2 produced during the experiment with acetone was obtained. This was a good indication of almost complete mineralization of acetone. Actually during the course of the first experiment without acetone the only by-products that could be detected by PID was acetone (maximum concentration 35 ppbV) and acetaldehyde (maximum concentration 85 ppbV). During the experiment with acetone, the only by-product detected by FID was acetaldehyde (maximum concentration 400 ppbV). No formaldehyde determination was performed but it may be assumed that a similar concentration to that of acetaldehyde was produced. In both experiments, air sampling on cartridges and thermo-desorption on ATD-GC-MS confirmed the absence of any other by-product than acetaldehyde.

All the films were compared under the same conditions and the apparent zero order kinetic constants for CO_2 production and acetone mineralization were determined by unit surface area (ppmV min^{-1} cm^{-2}) by dividing the experimentally calculated slopes by 600 cm^2.

In Fig. 8, the apparent kinetic constant are represented as a function of TiO_2 surface density. There was no clear correlation between this parameter and the rate constant of acetone

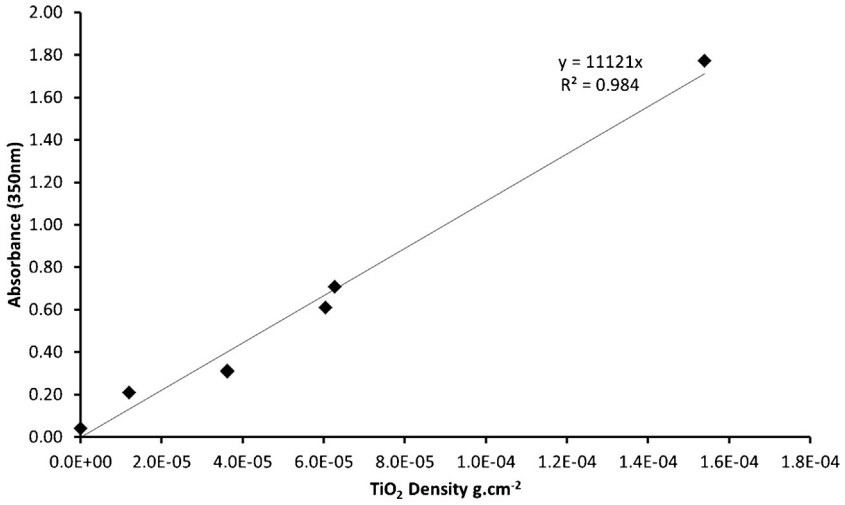

Fig. 6. Correlation between the intensity of the absorption band of the films at 350 nm and the surface density of TiO_2 (see Section 2).

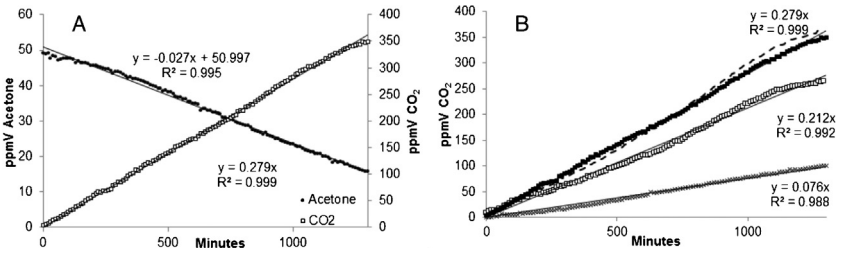

Fig. 7. Efficiency of the T3L/15/4.5 film for acetone degradation: (A) decrease of acetone concentration and increase of CO_2 concentration upon irradiation at 350 nm of a $30 \times 20\,cm^2$ film in the 1.17 m^3 closed chamber. (B) Increase of CO_2 concentration upon irradiation of the film without acetone (open square), with acetone (black square), calculated CO_2 concentrations deduced from acetone concentration decrease with 1 mole acetone giving 3 moles of CO_2 (cross). The dotted line corresponds to the addition of theoretical CO_2 produced by acetone mineralization and by the film decomposition itself.

degradation (Fig. 8C) even if the highest TiO_2 surface density gave the highest acetone degradation constant. It was also noticed that up to $4.05 \times 10^{-5}\,g\,TiO_2\,cm^{-2}$, there was no significant diffence between CO_2 production with or without acetone since the CO_2 production by the film alone is much higher than the CO_2 evolved from acetone mineralization. Under these conditions, the photocatalytic activity of the film was hardly evaluated. As smartly suggested by a reviewer, the production of acetone as an intermediate product starting from 2-propanol as a reference pollutant could allow the distinction between the degradation of the air pollutant (2-propanol) and the degradation of the films. However, these experiments were not carried out due to lack of time. Only for the two most loaded films (T3L/15/4.5 and T3L/50/3.3), the acetone degradation was sufficient to induce a significant difference between the CO_2 production in the two experiments. On the contrary, the two colored films W4L/13/3 and B5L/13/3 gave an almost negligeable degradation of acetone ($k_{acetone} = 0.2 \times 10^{-5}\,ppmV\,min^{-1}\,cm^{-2}$) and no significant difference of CO_2 production without or with added acetone. These films were thus inefficient for acetone mineralization, probably due to the presence of the pigmented layer ((4) in Fig. 1) which probably strongly reduced acetone diffusion to the photocatalytic layer.

DMDS degradation was studied in a small closed chamber with an external irradiation and without optimizing the transfer of DMDS on the film to reproduce fumigation conditions in wide fields. In this case, two experiments were successively carried out with the same film under 70% RH, the first one without added DMDS to monitor the film degradation by CO_2 evolution and the second one with added DMDS (Fig. 9B). As previously the box was flushed with fresh air between the two experiments. In the absence of DMDS, a significant CO_2 evolution was observed but there was an induction delay before CO_2 concentration increased linearly with time. The delay time may probably be related to the less efficient mass transfer of gaseous compounds in this device, inducing a slower monitoring of evolved CO_2 by the gas chromatograph. The apparent zero order kinetic constant k_{CO_2} was thus determined between 1 000 and 3 000 min ($k_{CO_2} = 0.298\,ppm\,Vmin^{-1}$, Fig. 9B open squares). A delay time was also noticed in the second experiment with added DMDS but the apparent kinetic constant deduced from the latter points of the curve was not very different from the previous one ($k_{CO_2} = 0.302\,ppm\,Vmin^{-1}$, Fig. 9B black squares). It was deduced that CO_2 arising from the expected mineralization of DMDS (Fig. 9A) was much lower than the CO_2 issued from the film degradation. When adding the curve of theoretical CO_2 to that obtained without DMDS a poorer agreement than with acetone (Fig. 7B) was obtained (Fig. 9B, dotted line). It was concluded that DMDS mineralization was not complete under these conditions after 60 h irradiation as confirmed by the ATD-GC-MS of sampled air and ionic chromatography of water used to wash the films after the experiment. ATD-GC-MS of sampled air only showed the main presence of traces of sulfur dioxide and carbon disulfide together with remaining DMDS (not quantified but undetectable on micro-TCD). Still lower amounts of other compounds such as acetic acid, dimethyltrisulfide, S-methyl methane thiosulfonate,

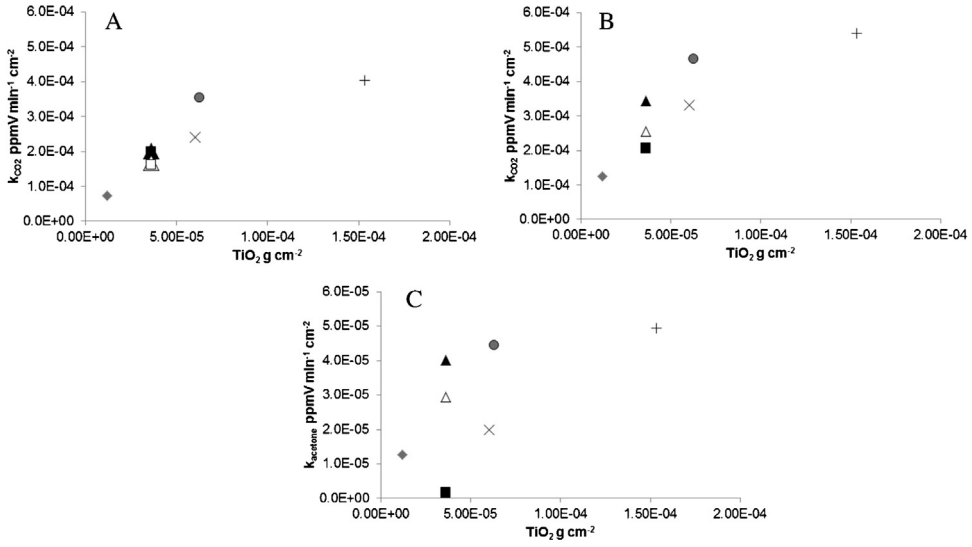

Fig. 8. Apparent kinetic constants for CO_2 production: (A) without acetone; (B) with acetone and (C) apparent kinetic constant for acetone degradation upon irradiation at 350 nm of a $30 \times 20\,cm^2$ film in the $1.2\,m^3$ closed chamber as function of TiO_2 density ($g\,cm^{-2}$). ♦: Film T3L/13/1; ▲: film T3L/13/3MB1; △: Film T3L/13/3MB2; □: film W4L/13/3; ■:: film B5L/13/3; ×: film T3L/50/1.3; ●: film T3L/15/4.5; +: film T3L/50/3.3.

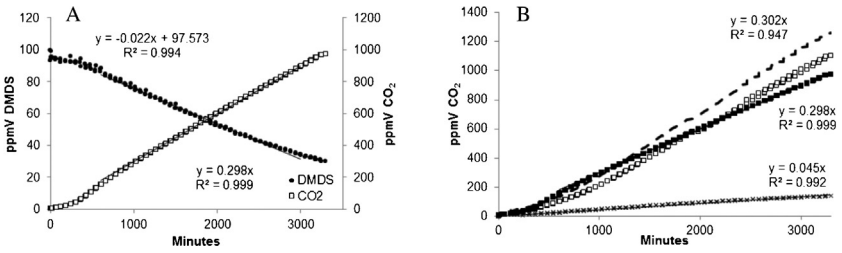

Fig. 9. Efficiency of the T3L/15/4.5 film for DMDS degradation: (A) decrease of DMDS concentration and increase of CO_2 concentration upon irradiation at 350 nm of a $20 \times 20\,cm^2$ film in the 144 L closed chamber. (B) increase of CO_2 concentration upon irradiation of the film without DMDS (open square), with DMDS (black square), calculated CO_2 concentrations deduced from DMDS concentration decrease with 1 mole DMDS giving 2 moles of CO_2 (cross). The dotted line corresponds to the addition of theoretical CO_2 produced by DMDS mineralization and by the film decomposition itself.

methyl(methylthio)methyl disulfide, methane sulfonic anhydride could only be detected when using much higher inlet DMDS concentration (25 000 ppmV). However, methyl sulfonate and sulfate were quantified in the washing water of the films irradiated with 100 ppmV DMDS. Their respective yields were for instance 4 and 10% with the film B5L/13/3 relative to introduced DMDS. However it should be stressed that at the end of these experiments, the walls of the whole box were covered with non volatile gummy liquid products that could not be washed and analyzed but probably also contained CH_3SO_3H and H_2SO_4. Complementary XPS analysis of the films after irradiation (ESI, Fig. S4) confirmed the presence of oxidized sulfur assigned to sulfates (168.6 and 169.8 ev) and organic sulfonates (163.6 and 164.8 eV). The presence of sulfonates accounted for the poor mineralization yield of DMDS deduced from Fig. 9B but indicated that oxidation of DMDS took place on the films.

The apparent zero order kinetic constants of DMDS degradation and CO_2 production by unit surface area (ppmV min^{-1} cm^{-2}, obtained by dividing the experimentally calculated slopes by 400 cm^2) without and with added DMDS are summarized in Table 3 and the corresponding curves in Fig. 10. Due to the different conditions between the two experiments (irradiated film areas, sources (spectra and irradiance), air flow around the TiO_2 film, and mainly different geometrical arrangement of the films relative the source and to the fans), the apparent kinetic constant for CO_2 production in the absence of pollutant may not be compared (Tables 2 and 3). However in both cases, CO_2 evolution increased with TiO_2 surface density. For most samples, there was also no significant difference between CO_2 production without or with added DMDS, except for the most concentrated film T3L/50/3.3 (Fig. 10A and B). For all the samples between 1.21 and 6.28×10^{-5} g cm^{-2}, no general trend for k_{DMDS} could be deduced with very low values between 3.0 and 5.2 10^{-5} ppmV min^{-1} cm^{-2} (Fig. 10C) as for $k_{acetone}$ (between 1.3 and 4.0×10^{-5} ppmV min^{-1} cm^{-2}, Fig. 8C). As for acetone, a weak influence of the master batch could be observed, with T3L/13/3MB2 only slightly less efficient than T3L/13/3MB1. Significant DMDS degradation was only observed with the most loaded film T3L/50/3.3, together with a very high CO_2 production indicating an extensive degradation of the film, going on even when there was no more DMDS in the device.

For the less loaded films (up to 6.28 10^{-5} g cm^{-2}), no obvious trend was observed for both acetone and DMDS degradation, while for the most efficient one T3L/50/3.3, k_{DMDS} and $k_{acetone}$ were much larger (27.8 and 4.9×10^{-5} ppmV min^{-1} cm^{-2} respectively). It may also be noticed that the white W4L/13/3 and the black B5L/13/3 films remained as active as the corresponding transparent films for DMDS degradation while they were almost inactive for acetone degradation ($k_{acetone} = 0.2 \times 10^{-5}$ ppmV min^{-1} cm^{-2}; $k_{DMDS} = 3.3$–3.5 ppmV min^{-1} cm^{-2}).

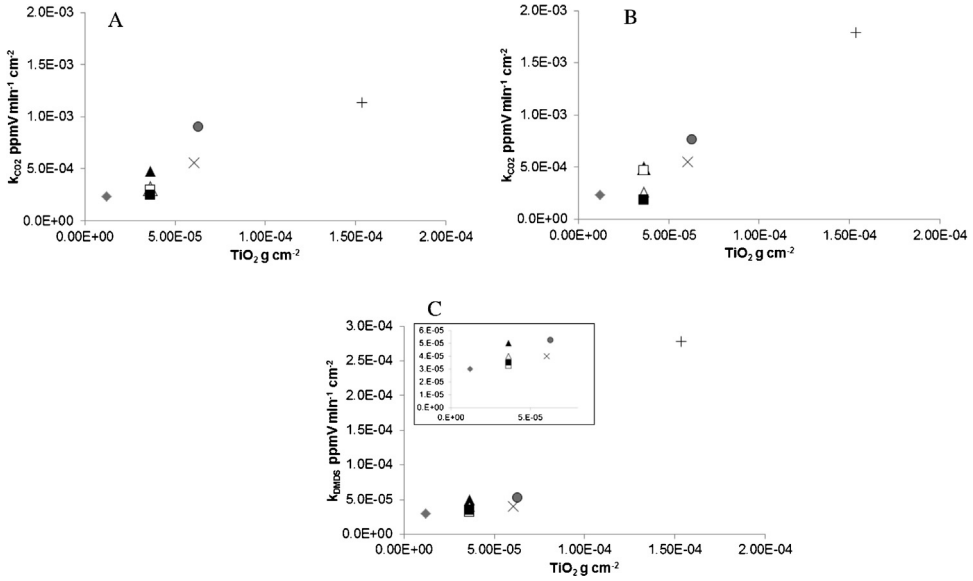

Fig. 10. Apparent zero order kinetic constants for CO_2 production (A) without DMDS; (B) with DMDS and (C) apparent kinetic constant for DMDS degradation upon irradiation at 350 nm of a $20 \times 20\,cm^2$ film in the 144 L closed chamber as function of TiO_2 density g cm^{-2}. ♦: Film T3L/13/1; ▲: film T3L/13/3MB1; △: film T3L/13/3MB2; □: film W4L/13/3; ■:: film B5L/13/3; ×: film T3L/50/1.3; ●: film T3L/15/4.5; +: film T3L/50/3.3.

Table 2
Apparent zero order kinetic constant of CO_2 formation without and with added acetone and of acetone degradation upon 365 nm irradiation of 600 cm^2 of the various photocatalytic films (size 30 × 20 cm^2).

Name	TiO_2 surface density (10^{-5} g cm^{-2})	k_{CO2} without acetone (10^{-4} ppmV min^{-1} cm^{-2})	k_{CO2} with acetone (10^{-4} ppmV min^{-1} cm^{-2})	$k_{acetone}$ (10^{-5} ppmV min^{-1} cm^{-2})
T3L/13/0	0			
T3L/13/1	1.21	0.7	1.3	1.3
T3L/13/3MB1	3.63	2.0	3.4	4.0
T3L/13/3MB2	3.6	1.7	2.6	2.9
W4L/13/3	3.63	1.6	2.0	0.2
B5L/13/3	3.63	2.0	2.1	0.2
T3L/50/1.3	6.05	2.4	3.3	2.0
T3L/15/4.5	6.28	3.5	4.7	4.5
T3L/50/3.3	15.3	4.0	5.4	4.9

Table 3
Zero order kinetic constant of CO_2 formation without and with added DMDS and of DMDS degradation upon 365 nm irradiation of 400 cm^2 of the various photocatalytic films (film size 40 × 40 cm^2).

Name	TiO_2 surface density (10^{-5} g cm^{-2})	k_{CO_2} without DMDS (10^{-4} ppmV min^{-1} cm^{-2})	k_{CO_2} with DMDS (10^{-4} ppmV min^{-1} cm^{-2})	k_{DMDS} (10^{-5} ppmV min^{-1} cm^{-2})
T3L/13/0	0			
T3L/13/1	1.21	2.4	2.4	3.0
T3L/13/3MB1	3.63	4.8	4.9	5.0
T3L/13/3MB2	3.6	3.1	2.6	4.0
W4L/13/3	3.63	3.0	4.7	3.3
B5L/13/3	3.63	2.5	1.9	3.5
T3L/50/1.3	6.05	5.6	5.5	4.0
T3L/15/4.5	6.28	9.0	7.6	5.3
T3L/50/3.3	15.3	11.4	17.9	27.8

4. Discussion

To the best of our knowledge, this is the first report of the elaboration of multilayer photocatalytic VIF films on an industrial scale, using commercial nanoparticulate TiO_2 blended in a PE master batch. From the detection of CO_2, acetone and acetaldehyde, our results clearly showed the decomposition of TiO_2-films under UV irradiation, in agreement with several previous studies. For instance, Thomas et al. [18] confirmed partial oxidation of PE TiO_2 films from their IR spectrum after UV irradiation showing the formation of carbonyl compounds. The study of the mechanism involved in the degradation of PE TiO_2 films was already addressed in numerous previous papers [11,13,21–24]. To limit the PE degradation, a protective SiO_2 layers was placed sandwich-like between the organic surface and the photocatalytic film [14]. Under our conditions, after 120 h of irradiation under UV A, all the multilayer films were still mechanically resistant and could be handled without problem although a white coloration of the photocatalytic layer was noticed (Fig. 11). It should be recalled that most of the previous studies on the photocatalytic efficiency of polymer-TiO_2 composites mainly addressed dye discoloration in solution, such as Orange II [13], Rhodamine B [25], or Methylene blue [26]. Two papers were devoted to gaseous pollutants oxidation: polyethylene terephthalate (PET) embedded TiO_2 was used for gaseous trichloroethylene (TCE) destruction [14], while TiO_2 incorporated in orthophtalic polyester polymers was also efficient for gaseous ethanol mineralization [27].

In the present study, for the most loaded film T3L/50/3.3, DMDS and acetone degradation was very efficient even it the apparent rate constants may not be simply compared due to different irradiation conditions. However acetone oxidation did not occur with the two white and black films, W4L/13/3 and B5L/13/3, while DMDS degradation was observed. A tentative explanation could be that the diffusion of acetone in the PE layer is less efficient than the diffusion of DMDS. In order to achieve efficient photocatalytic oxidation, molecules to be degraded have to diffuse in close vicinity of the TiO_2 particles. In case of the colored films, the pollutant molecules also have to diffuse through a supplementary PE colored layer, not favored in the case of acetone. Such a different permeability of PE films toward various fumigants has been already been reported [7]. We however demonstrated from the absence of by-products in significant amounts (only acetaldehyde at the ppbV level) that acetone mineralization was almost complete (*i.e.* all the degraded acetone is transformed into CO_2 and H_2O) with the most loaded films.

DMDS was also partially degraded but, in this case, several trace by-products were detected during the course of the reaction (SO_2, CS_2) and methanesulfonic acid was identified together with sulfuric acid as final products on the washed films and on the reactor walls. These results are consistent with the known photocatalytic oxidation of DMDS, which was already shown to be slower than that of dimethylsulfide either in the gas phase [28] or in solution [29]. Partial mineralization of DMDS on either ZnO or TiO_2, already reported by Guillard et al. in a flow-through reactor, mainly depended of the contact time and inlet DMDS concentration. Sulfates, but not

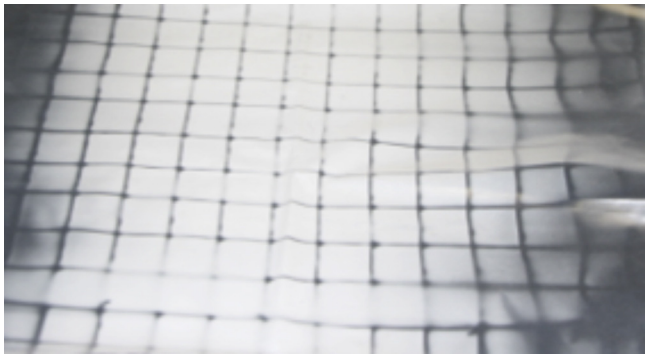

Fig. 11. Picture of the films after irradiation in the 1.2 m^3 closed chamber. The darker lines correspond to the metal frame used to support the film, which prevented them from light (color of the film before irradiation). The white zones were fully irradiated.

sulfur dioxide, were also detected by these authors at the end of these experiments, together with several organic intermediates [30]. SO_2 and sulfuric acid, the ultimate oxidation products of sulfur compounds, were detected during photocatalytic oxidation of H_2S on poly(ethylene)terephatlate-TiO_2 films [12]. Different glass- or polypropylene-supported rutile TiO_2 were also recently compared for gaseous DMDS oxidation but without indication of the oxidation products [31]. Under our lab conditions, irradiation of the films with UVA (similar irradiance to solar light) with DMDS lasted 3 600 min (60 h). The actual wide field use of such films will be at least 15 alternating night and day periods, corresponding roughly to 180 h of sun irradiation. It is thus expected that these increased irradiation times together with the digestion of the oxidation products by the soil will contribute to extensive DMDS degradation and to soil improvement due to oxidized sulfur uptake [32–34].

5. Conclusion

Industrial virtually impermeable films made of polyethylene (PE) and polyamide layers together with a photocatalytic layer prepared from a PE master batch containing commercial TiO_2 nanoparticles were prepared as transparent or colored fumigation films. The photocatalytic oxidation of dimethyl disulfide (DMDS), a large spectrum and efficient fumigant, was studied with these films. The aim was to define the optimal conditions to decrease DMDS concentration in the air space between the soil and the film at the end of the treatment in order to reduce the exposure of workers and neighborhood, while keeping an optimal DMDS concentration during the fumigation treatment. From the comparison between various films with different composition, number of layers, thickness and TiO_2 concentration it was concluded that for all the samples the light absorption was linearly correlated to TiO_2 surface density and that no further increase of TiO_2 content was necessary due to saturation of light absorption.

Acetone and DMDS mineralization was observed with most of the studied films, although different diffusion rates of acetone and DMDS inside the PE matrix was deduced from the comparison of the results with the colored black and white films. Under these laboratory conditions, DMDS mineralization was not complete since besides sulfates, methanesulfonate, as well as minute amounts of various oxidized products were detected in the air space and on the films at the end of the irradiation. In any case, DMDS and its oxidation products are known to be beneficial for plant growth [32–34].

It was thus demonstrated that these gastight photocatalytic films, colored or not, could be successfully used for wide field fumigation with DMDS and that by proper choice of the film composition and thickness, it was possible to optimize the DMDS degradation rate in the air space for maximum nematicide, fungicide and herbicide efficiency, with decreased buffer zones (area of no fumigation) and maximum safety for neighborhood and workers at the end of the treatment. Further wide fields studies based of these results are in progress.

Appendix A. Supplementary data

Supplementary material related to this article can be found, in the online version, at http://dx.doi.org/10.1016/j.apcatb.2014.09.022.

References

[1] H.W. Lembright, Suppl. J. Nematol. 21 (1989) 632.
[2] United Nations Environment Programme, Ozone Secretariat, United Nations Environment Programme, Ozone Secretariat, Nairobi, Kenya, 2005.
[3] J.J. Heller, P. Sunder, P. Charles, J.J. Pommier, J. Fritsch, in: J. LopezMedina (Ed.), Vi Int. Strawb. Symp., Int. Soc. Horticultural Science, Leuven 1, 2009, pp. 953–956.
[4] S.K. Papiernik, S.R. Yates, D.O. Chellemi, J. Environ. Qual. 40 (2011) 1375.
[5] D. Wang, S.R. Yates, F.F. Ernst, J. Gan, W.A. Jury, Environ. Sci. Technol. 31 (1997) 3686.
[6] A. Minuto, G. Gilardi, M.L. Gullino, A. Garibaldi, Crop Prot. 18 (1999) 365.
[7] D.O. Chellemi, H.A. Ajwa, D.A. Sullivan, R. Alessandro, J.P. Gilreath, S.R. Yates, J. Environ. Qual. 40 (2011) 1204.
[8] P. Charles, T. Fouillet, Photocatalytic Film for Soil Fumigation, FR2979521 (A1), Abstract of corresponding document: WO2013030513 (A1) (2013).
[9] S. Malato, P. Fernández-Ibáñez, M.I. Maldonado, J. Blanco, W. Gernjak, Catal. Today 147 (2009) 1.
[10] J. Peral, X. Domènech, D.F. Ollis, J. Chem. Technol. Biotechnol. 70 (1997) 117.
[11] Y. Zhiyong, E. Mielczarski, J. Mielczarski, D. Laub, P. Buffat, U. Klehm, P. Albers, K. Lee, A. Kulik, L. Kiwi-Minsker, A. Renken, J. Kiwi, Water Res. 41 (2007) 862.
[12] R. Portela, B. Sánchez, J.M. Coronado, R. Candal, S. Suárez, Catal. Today 129 (2007) 223.
[13] Y. Zhiyong, D. Laub, M. Bensimon, J. Kiwi, Inorg. Chim. Acta 361 (2008) 589.
[14] B. Sánchez, J.M. Coronado, R. Candal, R. Portela, I. Tejedor, M.A. Anderson, D. Tompkins, T. Lee, Appl. Catal. B: Environ. 66 (2006) 295.
[15] S. Singh, H. Mahalingam, P.K. Singh, Appl. Catal. Gen. 462–463 (2013) 178.
[16] C. Chawengkijwanich, Y. Hayata, Int. J. Food Microbiol. 123 (2008) 288.
[17] H. Bodaghi, Y. Mostofi, A. Oromiehie, Z. Zamani, B. Ghanbarzadeh, C. Costa, A. Conte, M.A. Del Nobile, LWT – Food Sci. Technol. 50 (2013) 702.
[18] R.T. Thomas, V. Nair, N. Sandhyarani, Colloids Surf. Physicochem. Eng. Asp. 422 (2013) 1.
[19] B. Kartheuser, N. Costarramone, T. Pigot, S. Lacombe, Environ. Sci. Pollut. Res. 19 (2012) 3763.
[20] M. Jeanmougin, J. Civatte, Ann. Dermatol. Venereol. 114 (1987) 671.
[21] X. u Zhao, Z. Li, Y. Chen, L. Shi, Y. Zhu, J. Mol. Catal. A: Chem. 268 (2007) 101.
[22] S.S. Fernando, P.A. Christensen, T.A. Egerton, J.R. White, Polym. Degrad. Stab. 92 (2007) 2163.
[23] L. Zan, W. Fa, S. Wang, Environ. Sci. Technol. 40 (2006) 1681.
[24] B. Ohtani, S. Adzuma, S. Nishimoto, T. Kagiya, Polym. Degrad. Stab. 35 (1992) 53.
[25] Y. Zhang, S. Wei, H. Zhang, S. Liu, F. Nawaz, F.-S. Xiao, J. Colloid Interface Sci. 339 (2009) 434.
[26] S. Naskar, S. Arumugom Pillay, M. Chanda, J. Photochem. Photobiol. Chem. 113 (1998) 257.
[27] M.P. Paschoalino, J. Kiwi, W.F. Jardim, Appl. Catal. B: Environ. 68 (2006) 68.
[28] H. Nishikawa, Y. Takahara, J. Mol. Catal. A: Chem. 172 (2001) 247.
[29] S. Lacombe, H. Cardy, M. Simon, A. Khoukh, J.P. Soumillion, M. Ayadim, Photochem. Photobiol. Sci. 1 (2002) 347.
[30] C. Guillard, D. Baldassare, C. Duchamp, M.N. Ghazzal, S. Daniele, Catal. Today 122 (2007) 160.
[31] L.-C. Chuang, C.-H. Luo, Mater. Res. Bull. 48 (2013) 238.
[32] D.G. Meldau, S. Meldau, L.H. Hoang, S. Underberg, H. Wünsche, I.T. Baldwin, Plant Cell 25 (2013) 2731.
[33] F.-Y. Wang, Q.-X. Wang, D.-D. Yan, L.-G. Mao, M.-X. Guo, P.-M. Yan, A.-C. Cao, Chin. J. Eco-Agric. 19 (2011) 890.
[34] G. Darracq, A. Couvert, C. Couriol, A. Amrane, P. Le Cloirec, Water Sci. Technol. 59 (2009) 1315.